Extracellular reactive oxygen species drive apoptosis-induced proliferation via drosophila macrophages

Fogarty, Caitlin E; Diwanji, Neha; Lindblad, Jillian L; Tare, Meghana; Amcheslavsky, Alla; Makhijani, Kalpana; Brückner, Katja; Fan, Yun; Bergmann, Andreas

DOI:
10.1016/j.cub.2015.12.064

Document Version
Peer reviewed version

Citation for published version (Harvard):
Fogarty, CE, Diwanji, N, Lindblad, JL, Tare, M, Amcheslavsky, A, Makhijani, K, Brückner, K, Fan, Y & Bergmann, A 2016, 'Extracellular reactive oxygen species drive apoptosis-induced proliferation via drosophila macrophages', Current Biology. https://doi.org/10.1016/j.cub.2015.12.064

Extracellular Reactive Oxygen Species drive Apoptosis-induced Proliferation via *Drosophila* Macrophages

Running title: ROS mediate apoptosis-induced proliferation

Caitlin E. Fogarty[1,4], Neha Diwanji[1,4], Jillian L. Lindblad[1,4], Meghana Tare[1,4], Alla Amcheslavsky[1,4], Kalpana Makhijani[2], Katja Brückner[2], Yun Fan[3] and Andreas Bergmann[1,5]

[1] University of Massachusetts Medical School
Department of Molecular, Cell and Cancer Biology
364 Plantation Street – LRB 416
Worcester, MA 01605
USA

[2] University of California San Francisco
Broad Center, Department of Cell and Tissue Biology
35 Medical Center Way
San Francisco CA, 94143
USA

[3] University of Birmingham
School of Biosciences
Edgbaston
Birmingham, B15 2TT
UK

[4] Co-first authors

[5] Corresponding author: Andreas.Bergmann@umassmed.edu
Tel. +1 508.856.6423

Summary

Apoptosis-induced proliferation (AiP) is a compensatory mechanism to maintain tissue size and morphology following unexpected cell loss during normal development, and may also be a contributing factor to cancer and drug resistance. In apoptotic cells, caspase-initiated signaling cascades lead to the downstream production of mitogenic factors and the proliferation of neighbouring surviving cells. In epithelial cells of *Drosophila* imaginal discs, the Caspase-9 ortholog Dronc drives AiP via activation of Jun N-terminal kinase (JNK); however, the specific mechanisms of JNK activation remain unknown. Here, we show that caspase-induced activation of JNK during AiP depends on an inflammatory response. This is mediated by extracellular reactive oxygen species (ROS) generated by the NADPH oxidase Duox in epithelial disc cells. Extracellular ROS activate *Drosophila* macrophages (hemocytes), which in turn trigger JNK activity in epithelial cells by signaling through the TNF ortholog Eiger. We propose that in an immortalized ('undead') model of AiP, signaling back and forth between epithelial disc cells and hemocytes by extracellular ROS and TNF/Eiger drives overgrowth of the disc epithelium. These data illustrate a bidirectional cell/cell communication pathway with implication for tissue repair, regeneration and cancer.

Introduction

Following significant apoptotic cell death, apoptosis-induced proliferation (AiP) is a form of compensatory proliferation that can regenerate lost tissue via additional or accelerated cell divisions and is defined as the process by which apoptotic cells actively stimulate surviving cells to divide [1]. In *Drosophila*, there is mounting evidence that AiP is driven by mitogenic signals produced by apoptotic caspases in the dying cell [2-8]. Likewise, numerous studies in several regenerative model organisms including Hydra, planarians, newt, zebrafish, Xenopus and mammals have validated the concept of caspase-driven AiP (reviewed in [9, 10]). Furthermore, AiP may also be a contributing factor for the development of cancer and drug resistance [11-14].

Caspases are highly specific cell death proteases. In apoptotic cells, activated initiator caspases such as Caspase-9 and its *Drosophila* ortholog Dronc cleave and activate effector caspases such as Caspase-3 and its orthologs DrICE and Dcp-1 which trigger apoptosis (reviewed in [9, 10]). In addition to activating effector caspases, Dronc can also promote AiP through activation of Jun N-terminal kinase (JNK) signaling [4, 5, 15-18]. However, the specific mechanisms by which Dronc activates JNK are not known. Therefore, to facilitate screening for genes and mechanisms involved in AiP, we have developed the *ey>hid-p35* model in *Drosophila* [5]. In this AiP model, the pro-apoptotic gene *hid* and the caspase inhibitor *p35* are co-expressed under control of the *eyeless-Gal4* (*ey-Gal4*) driver in the anterior eye imaginal disc. Because P35 very specifically inhibits the effector caspases DrICE and Dcp-1 in *Drosophila* [19], *hid*/*p35*-expressing cells initiate the apoptotic process by activating Dronc, but cannot execute apoptosis due to effector caspase inhibition by P35, thus producing "undead" cells [2-5, 15]. Furthermore, because undead cells do not die, continued Dronc signaling initiates a feedback amplification loop that involves Dronc, JNK and Hid which further amplifies the signals for AiP [16, 20].

Thus, Dronc chronically signals for AiP and triggers overgrown imaginal discs which in the case of *ey>hid-p35* produces overgrowth of adult heads with pattern duplications compared to control (*ey>p35*) animals (Figure 1A,B) [5]. In *ey>hid-p35* eye imaginal discs, the anterior part of the eye disc where *ey-Gal4* is expressed is overgrown at the expense of the posterior eye field [5]. This reduction of the posterior eye field can be visualized using the photoreceptor marker ELAV (Figure S1A,B). We are using the normalization of the ELAV pattern in the posterior eye field in various genetic backgrounds as indicator of the suppression of *ey>hid-p35*–induced overgrowth at the disc level (Figure S1C).

Here, using the *ey>hid-p35* model of AiP to investigate the mechanisms by which Dronc activates JNK signaling, we show that Dronc activity in epithelial disc cells promotes activation of the NADPH oxidase Duox which generates extracellular reactive oxygen species (ROS). Extracellular ROS activate hemocytes, *Drosophila* macrophages, at undead tissue. Activated hemocytes in turn release the TNF ligand Eiger which promotes JNK activation in epithelial cells and promotes AiP. These data illustrate a bidirectional cell/cell communication pathway with implication for tissue repair, regeneration and cancer.

Results

Ectopic production of ROS in apoptosis-induced proliferation

When reactive oxygen species (ROS) accumulate indiscriminately within cells, they can be toxic leading to oxidative stress and possible cell death. However, at lower, controlled levels, ROS can have specific roles in growth control, proliferation and differentiation [21]. Recent studies have demonstrated critical requirements for ROS during wound healing and regeneration, and in certain contexts via activation of JNK [22-24]. In order to examine the role of ROS in

AiP, we assessed *in vivo* ROS levels in *Drosophila* imaginal discs using the ROS-reactive dyes dihydroethidium (DHE) and the fluorescein based H_2-DCF-DA [25]. In undead eye imaginal discs, ROS are dramatically increased compared to control discs (Figure 1D,E,H,I). This increased ROS production in undead tissue is dependent on Dronc activity (Figure 1F,J) consistent with the suppression of the adult head overgrowth phenotype (Figure 1C) and the normalization of the ELAV pattern by *dronc* mutations (Figure S1C). We also detected increased ROS in undead wing imaginal discs (*nub>hid-p35*) (Figure 1L,M) suggesting that the production of ROS in response to caspase activation is not tissue-specific. These data imply that ROS can be generated in developing epithelial tissues following initiator caspase activation, independently of cell death execution.

We also examined if ROS are produced in a *p35*-independent AiP model in which apoptosis is temporally induced and cells are allowed to die [5, 17, 18, 26]. In this AiP model, *hid* expression is induced for 12h in the dorsal half of the eye disc using *dorsal eye*-(*DE-)Gal4* (*DE^{ts}>hid*) during 2nd or 3rd larval instar [5]. ROS are observed immediately after apoptosis induction (Figure 1N,O; Figure S2A,D) suggesting that its production is an early event in the death and regeneration process. In this AiP model, ROS levels can be detected for up to 24 hours after apoptosis induction (Figure S2B,C). These data are consistent with a recent report about ROS production in a *p35*-independent model in wing imaginal discs [27].

Extracellular ROS are required for apoptosis-induced proliferation upstream of JNK

To determine if there is a functional requirement for ROS in AiP, we mis-expressed ROS-reducing enzymes in the undead AiP model. However, mis-expression of cytosolic SOD and cytosolic catalase transgenes did not significantly suppress *ey>hid-p35*-induced overgrowth

(Figure 2A,E). In contrast, mis-expression of two extracellular catalases, *immune-regulated catalase* (*IRC*) and a secreted human catalase (*hCatS)*, does suppress *ey>hid-p35*-induced overgrowth (Figure 2B,E; see detailed statistical analysis in Figure S3F). Consistently, mis-expression of *hCatS* results in a strong reduction of ROS in undead eye discs (Figure S3A-C). These observations suggest that extracellular ROS are required for AiP following induction of apoptosis.

Two enzymes known to generate extracellular ROS are the transmembrane NADPH oxidases Nox and Duox [28]. To examine if either of these enzymes are involved in ROS production during AiP, we knocked down their expression by RNAi. Targeting *Nox* did not significantly suppress the AiP overgrowth phenotype in *ey>hid-p35* animals (Figure 2C,E; see summary in Figure S3E). In contrast, RNAi against *Duox* produced a suppression of the AiP overgrowth phenotype (Figure 2D,E; Figure S3D,E). Three independent RNAi transgenes for both of these genes gave consistent results (Figure S3D,E).

Because *ey>hid-p35* imaginal discs cause overgrowth due to increased cell proliferation (Figure 2F) [5], we examined if the suppression of overgrowth by *Duox* RNAi and *hCatS* expression is due to reduction of mitotic activity in *ey>hid-p35* discs by PH3 labeling. This was indeed found to be the case (Figure 2G",H",I"; quantified in Figure 2F). Concomitantly, a normalization of the ELAV pattern was observed in *ey>hid-p35* discs after reduction of ROS by *Duox* RNAi and *hCatS* expression (Figure 2G-I).

As *Duox* was disc-autonomously inhibited in undead cells (using *ey-Gal4*), these data indicate that extracellular ROS originate from the same cells that have activated Dronc, consistent with the observation that ROS production requires Dronc (Figure 1F,G,J,K).

Combined, Duox activity in undead cells produces extracellular ROS, which is required for AiP-induced overgrowth.

Next, we examined the position of ROS function relative to JNK, which is a critical mediator of AiP [4, 5, 17, 18]. Using MMP1 as a marker of JNK activity [29], we observed that JNK activity is strongly reduced in undead eye discs that overexpress *hCatS* or *Duox* RNAi (Figure 2G'-I'). Furthermore, activation of JNK by overexpression of a constitutively active JNKK (hep^{CA}) in a $dronc^{-/-}$ background does not result in the generation of ROS (Figure S4). These data are consistent with a model in which extracellular ROS are produced and acting upstream of JNK. Because JNK markers and cleaved Caspase 3 labelings overlap in undead cells [4, 5, 18], we propose that extracellular ROS signal back to undead cells – directly or indirectly - to turn on JNK, and thus activate downstream mitogen production for AiP.

ROS activate hemocytes for apoptosis-induced proliferation

To identify the function of extracellular ROS, we considered that they may activate hemocytes, *Drosophila* innate immune cells, as has been observed in *Drosophila* embryos [30]. Indeed, the pan-hemocyte anti-Hemese (H2) antibody [31] revealed that hemocytes are attached to both control and undead eye imaginal discs (Figure 3A,B). In wing imaginal discs, where no hemocytes are attached to control discs, there is a strong increase in the number of hemocytes attached to undead tissue (Figure S5A,B). There are three different types of hemocytes in the *Drosophila* larva: plamatocytes, lamellocytes and crystal cells [32]. Cell type-specific markers identify the hemocytes attached to undead tissue as macrophage-like plasmatocytes (Figure S5C-E).

Most strikingly, although hemocytes are present at control eye imaginal discs, they change morphology and location when they are attached to undead tissue. At control eye discs, they tend to form large cell clusters (Figure 3A,C) which are located around the border between anterior proliferating tissue and the posterior differentiating photoreceptors. In contrast, hemocytes on undead discs are enlarged and often present as single cells, are less spherical and extent cellular protrusions (Figure 3B,D) which may assist in signaling between hemocytes and undead epithelial cells [33]. Furthermore, they also attach to undead tissue that displaces part of the posterior eye tissue as visualized by disrupted ELAV labeling (compare Figure 3B,B' with 3A,A'). A similar morphology of activated hemocytes was observed in undead wing imaginal discs (Figure S5B). Upon loss of ROS by expression of the extracellular catalase *hCatS* or *Duox* RNAi, hemocyte recruitment is strongly impaired and ELAV labeling is normalized (Figure 3E,F). These results suggest that extracellular ROS activate hemocytes at undead tissue.

Interestingly, we also noted that the labeling of *ey>hid-p35* discs with cleaved caspase-3 antibody (CC3) is reduced, but not completely absent, when ROS are removed by *Duox* RNAi and *hCatS* expression (compare Figure 3E",F" with 3B"). Because CC3 is a marker of active Dronc [34] which is activated by *ey*-driven *hid*, and because CC3 labeling is not completely absent, the reduction of CC3 labeling after removal of extracellular ROS suggest that ROS participate in the feedback amplification loop between Dronc, JNK and Hid that has previously been described during stress-induced apoptosis [16, 20].

Hemocytes are required for apoptosis-induced proliferation

Next, we investigated whether hemocytes promote or restrict the overgrowth of undead tissue. To address this question, we analyzed *ey>hid-p35* animals that are mutant for *serpent*

(*srp*), a GATA-type Zn-finger transcription factor that is required for hemocyte differentiation [35]. Of particular importance is the srp^{neo45} allele that specifically affects *srp*'s requirement for hemocyte differentiation, but leaves other functions of *srp* intact [36]. The adult overgrowth phenotype of *ey>hid-p35* animals is dramatically suppressed when heterozygous mutant for srp^{neo45} (Figure 4A,B,E; see detailed statistics in Figure S3G). Similar results were obtained for a different *srp* allele, srp^{01549} (Figure 4C,E; Figure S3G). In contrast, inactivation of *srp* specifically in the eye imaginal disc epithelium using three independent RNAi lines does not result in suppression of the overgrowth phenotype (Figure 4D,E; Figure S3G) indicating that *srp* is required non-disc autonomously for AiP. Given that srp^{neo45} specifically affects hemocyte function, we conclude that hemocytes are required for AiP in the *ey>hid-p35* model.

Concomitantly, loss of *srp* function reduces JNK activity in undead tissue (Figure 4F,G,H). To exclude the possibility that JNK activity is responsible for hemocyte recruitment to undead disc tissue, we activated JNK by expression of hep^{CA}. This experiment was done in a $dronc^{-/-}$ background to block the feedback amplification loop which may otherwise activate hemocytes. However, under these conditions, hemocytes are not activated (Figure S6) further substantiating that hemocytes are acting upstream of JNK. These results suggest that undead tissue produces extracellular ROS through activation of Duox, which triggers an inflammatory response by activating hemocytes. Hemocytes in turn are required for JNK activation and the overgrowth of the undead epithelial disc tissue.

Interestingly, *ey>hid-35* eye discs mutant for *srp* also show a reduction, but not complete absence, of caspase activity as detected by CC3 (Figure 4I,J,K). This observation suggests that hemocytes participate in the feedback amplification loop in apoptotic cells described previously [16, 20].

Hemocytes activate JNK through the TNF system Eiger/Grindelwald

We frequently observed that hemocytes and epithelial cells expressing the JNK marker *puc-lacZ* are in direct contact (Figure 5A), further confirming the notion that hemocytes promote JNK activation in epithelial disc cells. This observation suggests that hemocytes release one or more signals that induce JNK activation in disc cells and promote AiP.

One signal known to induce the JNK cascade in epithelial cells is Eiger, a TNF-like ligand in *Drosophila* [37-39]. To test a requirement of Eiger for AiP, we generated *ey>hid-p35* flies in homozygous *eiger* mutant background. Under these conditions, the overgrowth of the adult head is strongly suppressed (Figure 5B,C,E; see detailed statistical analysis in Figure S3H). Loss of *eiger* also results in loss of JNK activity in *ey>hid-p35* discs (Figure 5F,G,G',H,H') consistent with a role of Eiger signaling for JNK activation [37-39].

In contrast, RNAi targeting *eiger* specifically in the eye disc (using *ey-Gal4*), does not suppress the overgrowth phenotype [5] (Figure 5E; Figure S3H) suggesting a non-disc autonomous function of Eiger. A putative role of Eiger in hemocytes is supported by immunofluorescent analysis using anti-Eiger antibody. In contrast to *ey>p35* controls, we observed Eiger protein in hemocytes attached to undead epithelial tissue (Figure 6; arrows in D and D'). There is also increased diffused Eiger labeling immediately outside of hemocytes at undead disc tissue (arrowhead in Figure 6D',D"). These data suggest that Eiger is upregulated in and secreted by hemocytes attached to undead tissue consistent with work by another group which showed increased Eiger protein in hemocytes in a different context [40].

There are two putative Eiger/TNF receptors encoded in the *Drosophila* genome, *wengen* and *grindelwald* (*grnd*) [39, 41, 42]. We have previously shown that *wengen* is not required disc-autonomously for overgrowth of undead tissue [5] (see also Figure 5E; Figure S3H). In contrast, RNAi targeting *grnd* in the disc strongly suppressed the overgrowth of *ey>hid-p35* animals (Figure 5D,E; Figure S3H) suggesting a disc-autonomous requirement of *grnd*. Consistently, Grnd uses the same regulatory factors for JNK activation, Traf2 and Tak1 [42], that are also required for JNK activation in AiP [5]. Additionally, upon *grnd* knockdown, the ectopic JNK activity in the undead tissue is lost (Figure 5I). These results provide evidence that Eiger/Grnd-dependent activation of JNK serves as intermediary of hemocyte/disc crosstalk, which is required for AiP and overgrowth of undead epithelial tissue.

Discussion

The role of ROS as a regulated form of redox signaling in damage detection and damage response is becoming increasingly clear [21]. Here, we have shown that in *Drosophila* extracellular ROS generated by the NADPH oxidase Duox drive compensatory proliferation and overgrowth following *hid*-induced activation of the initiator caspase Dronc in developing epithelial tissues (Figure 7). We find that at least one consequence of ROS production is the activation of hemocytes at undead epithelial disc tissue. Furthermore, our work implies that extracellular ROS and hemocytes are part of the feedback amplification loop between Hid, Dronc and JNK (Figure 7) that occurs during stress-induced apoptosis [16, 20]. Finally, hemocytes release the TNF ligand Eiger which promotes JNK activation in epithelial disc cells (Figure 7).

This work helps to understand why JNK activation occurs mostly in apoptotic/undead cells, but occasionally also in neighbouring surviving cells [4, 5, 17, 18]. Because our data indicate that hemocytes trigger JNK activation in epithelial cells, the location of hemocytes on the imaginal discs determines which epithelial cells receive the signal for JNK activation (Figure 7). Nevertheless, we do not exclude the possibility that there is also an autonomous manner of Dronc-induced JNK activation in undead/apoptotic cells as indicated in Figure 7.

In the context of apoptosis, hemocytes engulf and degrade dying cells [43]. However, there is no evidence that hemocytes have this role in the undead AiP model. We do not observe CC3 material in hemocytes attached to undead tissue. Therefore, the role of hemocytes in driving proliferation is less clear and likely context-dependent. In *Drosophila* embryos, hemocytes are required for epidermal wound healing, but this is a non-proliferative process [24]. With respect to tumor models in *Drosophila*, much of the research to date has focused on the tumor suppressing role of hemocytes and the innate immune response [44-46]. However, a few reports have implicated hemocytes as tumor-promoters in a neoplastic tumor model [40, 47]. Consistently, in our undead model of AiP, we find that hemocytes have an overgrowth- and tumor-promoting role. Therefore, the state of the damaged tissue and the signals produced by the epithelium may have differential effects on hemocyte response.

In a recent study, ROS were found to be required for tissue repair of wing imaginal discs in a regenerative (*p35*-independent) model of AiP [27], consistent with our work. While a role of hemocytes was not investigated in this study [27], it should be noted that *p35*-independent AiP models do not cause overgrowth, while undead ones like the *ey>hid-p35* AiP model do. It is therefore possible that ROS in *p35*-independent AiP models are necessary for tissue repair independently of hemocytes, while ROS in conjunction with ROS-activated hemocytes in

undead models mediate the overgrowth of the affected tissue. Future work will clarify the overgrowth-promoting function of hemocytes. These considerations are reminiscent of mammalian systems, where many solid tumors are known to host alternatively activated (M2) tumor-associated macrophages, which promote tumor growth and are associated with a poor prognosis (reviewed in [48]).

As tumors are considered "wounds that do not heal" [49], we see the undead model of AiP as a tool to probe the dynamic interactions and intercellular signaling events that occur in the chronic wound microenvironment. Future studies will investigate the specific mechanisms of hemocyte-induced growth and the tumor promoting role of inflammation in *Drosophila* as well as roles of additional tissue types, such as the fat body, on modulating tumorous growth.

Experimental Procedures

See Supplemental Information for experimental procedures.

Author contributions

AB supervised the project. CEF, ND, MT, JLL and AA carried out most of the experiments. KM, KB and YF provided essential reagents. CEF and AB discussed and interpreted the results and wrote the manuscript.

Acknowledgements

We would like to thank István Andó, Eric Baehrecke, Marc Freeman, Won Jae Lee, Masayuki Miura, Neal Silvermann, the Bloomington *Drosophila* Stock Center, the Vienna *Drosophila* Resource Center, and the Developmental Studies Hybridoma Bank for fly lines and reagents; Ernesto Perez for input and technical expertise; Latisha Eilijo for technical assistance. CEF would like to thank the UMMS MD/PhD program for ongoing support. This work was supported by a grant from the National Institute of General Medical Sciences (NIGMS) to AB.

References

1. Mollereau, B., Perez-Garijo, A., Bergmann, A., Miura, M., Gerlitz, O., Ryoo, H.D., Steller, H., and Morata, G. (2013). Compensatory proliferation and apoptosis-induced proliferation: a need for clarification. Cell death and differentiation *20*, 181.
2. Huh, J.R., Guo, M., and Hay, B.A. (2004). Compensatory proliferation induced by cell death in the Drosophila wing disc requires activity of the apical cell death caspase Dronc in a nonapoptotic role. Curr Biol *14*, 1262-1266.
3. Perez-Garijo, A., Martin, F.A., and Morata, G. (2004). Caspase inhibition during apoptosis causes abnormal signalling and developmental aberrations in Drosophila. Development *131*, 5591-5598.
4. Ryoo, H.D., Gorenc, T., and Steller, H. (2004). Apoptotic cells can induce compensatory cell proliferation through the JNK and the Wingless signaling pathways. Dev Cell *7*, 491-501.
5. Fan, Y., Wang, S., Hernandez, J., Yenigun, V.B., Hertlein, G., Fogarty, C.E., Lindblad, J.L., and Bergmann, A. (2014). Genetic models of apoptosis-induced proliferation decipher activation of JNK and identify a requirement of EGFR signaling for tissue regenerative responses in Drosophila. PLoS genetics *10*, e1004131.
6. Perez-Garijo, A., Shlevkov, E., and Morata, G. (2009). The role of Dpp and Wg in compensatory proliferation and in the formation of hyperplastic overgrowths caused by apoptotic cells in the Drosophila wing disc. Development *136*, 1169-1177.
7. Fan, Y., and Bergmann, A. (2008). Apoptosis-induced compensatory proliferation. The Cell is dead. Long live the Cell! Trends Cell Biol *18*, 467-473.
8. Fan, Y., and Bergmann, A. (2008). Distinct mechanisms of apoptosis-induced compensatory proliferation in proliferating and differentiating tissues in the Drosophila eye. Dev Cell *14*, 399-410.
9. Bergmann, A., and Steller, H. (2010). Apoptosis, stem cells, and tissue regeneration. Science signaling *3*, re8.
10. Ryoo, H.D., and Bergmann, A. (2012). The role of apoptosis-induced proliferation for regeneration and cancer. Cold Spring Harbor perspectives in biology *4*, a008797.

11. Huang, Q., Li, F., Liu, X., Li, W., Shi, W., Liu, F.F., O'Sullivan, B., He, Z., Peng, Y., Tan, A.C., et al. (2011). Caspase 3-mediated stimulation of tumor cell repopulation during cancer radiotherapy. Nature medicine *17*, 860-866.
12. Kurtova, A.V., Xiao, J., Mo, Q., Pazhanisamy, S., Krasnow, R., Lerner, S.P., Chen, F., Roh, T.T., Lay, E., Ho, P.L., et al. (2015). Blocking PGE2-induced tumour repopulation abrogates bladder cancer chemoresistance. Nature *517*, 209-213.
13. Donato, A.L., Huang, Q., Liu, X., Li, F., Zimmerman, M.A., and Li, C.Y. (2014). Caspase 3 promotes surviving melanoma tumor cell growth after cytotoxic therapy. The Journal of investigative dermatology *134*, 1686-1692.
14. Ford, C.A., Petrova, S., Pound, J.D., Voss, J.J., Melville, L., Paterson, M., Farnworth, S.L., Gallimore, A.M., Cuff, S., Wheadon, H., et al. (2015). Oncogenic properties of apoptotic tumor cells in aggressive B cell lymphoma. Curr Biol *25*, 577-588.
15. Kondo, S., Senoo-Matsuda, N., Hiromi, Y., and Miura, M. (2006). DRONC coordinates cell death and compensatory proliferation. Molecular and cellular biology *26*, 7258-7268.
16. Wells, B.S., Yoshida, E., and Johnston, L.A. (2006). Compensatory proliferation in Drosophila imaginal discs requires Dronc-dependent p53 activity. Curr Biol *16*, 1606-1615.
17. Bergantinos, C., Corominas, M., and Serras, F. (2010). Cell death-induced regeneration in wing imaginal discs requires JNK signalling. Development *137*, 1169-1179.
18. Herrera, S.C., Martin, R., and Morata, G. (2013). Tissue homeostasis in the wing disc of Drosophila melanogaster: immediate response to massive damage during development. PLoS genetics *9*, e1003446.
19. Meier, P., Silke, J., Leevers, S.J., and Evan, G.I. (2000). The Drosophila caspase DRONC is regulated by DIAP1. The EMBO journal *19*, 598-611.
20. Shlevkov, E., and Morata, G. (2012). A dp53/JNK-dependant feedback amplification loop is essential for the apoptotic response to stress in Drosophila. Cell death and differentiation *19*, 451-460.
21. Schieber, M., and Chandel, N.S. (2014). ROS function in redox signaling and oxidative stress. Curr Biol *24*, R453-462.
22. Gauron, C., Rampon, C., Bouzaffour, M., Ipendey, E., Teillon, J., Volovitch, M., and Vriz, S. (2013). Sustained production of ROS triggers compensatory proliferation and is required for regeneration to proceed. Scientific reports *3*, 2084.
23. Juarez, M.T., Patterson, R.A., Sandoval-Guillen, E., and McGinnis, W. (2011). Duox, Flotillin-2, and Src42A are required to activate or delimit the spread of the transcriptional response to epidermal wounds in Drosophila. PLoS genetics *7*, e1002424.
24. Razzell, W., Evans, I.R., Martin, P., and Wood, W. (2013). Calcium flashes orchestrate the wound inflammatory response through DUOX activation and hydrogen peroxide release. Curr Biol *23*, 424-429.
25. Owusu-Ansah, E., Yavari, A., and Banerjee, U. (2008). A protocol for *in vivo* detection of reactive oxygen species. Nature Protocols.
26. Smith-Bolton, R.K., Worley, M.I., Kanda, H., and Hariharan, I.K. (2009). Regenerative growth in Drosophila imaginal discs is regulated by Wingless and Myc. Dev Cell *16*, 797-809.
27. Santabarbara-Ruiz, P., Lopez-Santillan, M., Martinez-Rodriguez, I., Binagui-Casas, A., Perez, L., Milan, M., Corominas, M., and Serras, F. (2015). ROS-Induced JNK and p38 Signaling Is Required for Unpaired Cytokine Activation during Drosophila Regeneration. PLoS genetics *11*, e1005595.
28. Bae, Y.S., Choi, M.K., and Lee, W.J. (2010). Dual oxidase in mucosal immunity and host-microbe homeostasis. Trends in immunology *31*, 278-287.
29. Uhlirova, M., and Bohmann, D. (2006). JNK- and Fos-regulated Mmp1 expression cooperates with Ras to induce invasive tumors in Drosophila. The EMBO journal *25*, 5294-5304.

30. Moreira, S., Stramer, B., Evans, I., Wood, W., and Martin, P. (2010). Prioritization of competing damage and developmental signals by migrating macrophages in the Drosophila embryo. Curr Biol *20*, 464-470.
31. Kurucz, E., Zettervall, C.J., Sinka, R., Vilmos, P., Pivarcsi, A., Ekengren, S., Hegedus, Z., Ando, I., and Hultmark, D. (2003). Hemese, a hemocyte-specific transmembrane protein, affects the cellular immune response in Drosophila. Proceedings of the National Academy of Sciences of the United States of America *100*, 2622-2627.
32. Kurucz, E., Vaczi, B., Markus, R., Laurinyecz, B., Vilmos, P., Zsamboki, J., Csorba, K., Gateff, E., Hultmark, D., and Ando, I. (2007). Definition of Drosophila hemocyte subsets by cell-type specific antigens. Acta biologica Hungarica *58 Suppl*, 95-111.
33. Roy, S., and Kornberg, T.B. (2015). Paracrine signaling mediated at cell-cell contacts. BioEssays : news and reviews in molecular, cellular and developmental biology *37*, 25-33.
34. Fan, Y., and Bergmann, A. (2010). The cleaved-Caspase-3 antibody is a marker of Caspase-9-like DRONC activity in Drosophila. Cell death and differentiation *17*, 534-539.
35. Gold, K.S., and Bruckner, K. (2014). Drosophila as a model for the two myeloid blood cell systems in vertebrates. Experimental hematology *42*, 717-727.
36. Rehorn, K.P., Thelen, H., Michelson, A.M., and Reuter, R. (1996). A molecular aspect of hematopoiesis and endoderm development common to vertebrates and Drosophila. Development *122*, 4023-4031.
37. Moreno, E., Yan, M., and Basler, K. (2002). Evolution of TNF signaling mechanisms: JNK-dependent apoptosis triggered by Eiger, the Drosophila homolog of the TNF superfamily. Curr Biol *12*, 1263-1268.
38. Igaki, T., Kanda, H., Yamamoto-Goto, Y., Kanuka, H., Kuranaga, E., Aigaki, T., and Miura, M. (2002). Eiger, a TNF superfamily ligand that triggers the Drosophila JNK pathway. The EMBO journal *21*, 3009-3018.
39. Kauppila, S., Maaty, W.S., Chen, P., Tomar, R.S., Eby, M.T., Chapo, J., Chew, S., Rathore, N., Zachariah, S., Sinha, S.K., et al. (2003). Eiger and its receptor, Wengen, comprise a TNF-like system in Drosophila. Oncogene *22*, 4860-4867.
40. Cordero, J.B., Macagno, J.P., Stefanatos, R.K., Strathdee, K.E., Cagan, R.L., and Vidal, M. (2010). Oncogenic Ras diverts a host TNF tumor suppressor activity into tumor promoter. Dev Cell *18*, 999-1011.
41. Kanda, H., Igaki, T., Kanuka, H., Yagi, T., and Miura, M. (2002). Wengen, a member of the Drosophila tumor necrosis factor receptor superfamily, is required for Eiger signaling. The Journal of biological chemistry *277*, 28372-28375.
42. Andersen, D.S., Colombani, J., Palmerini, V., Chakrabandhu, K., Boone, E., Röthlisberger, M., Toggweiler, J., Basler, K., Mapelli, M., Hueber, A.-O., et al. (2015). The Drosophila TNF receptor Grindelwald couples loss of cell polarity with neoplastic growth. Nature *in press*.
43. Manaka, J., Kuraishi, T., Shiratsuchi, A., Nakai, Y., Higashida, H., Henson, P., and Nakanishi, Y. (2004). Draper-mediated and phosphatidylserine-independent phagocytosis of apoptotic cells by Drosophila hemocytes/macrophages. The Journal of biological chemistry *279*, 48466-48476.
44. Hauling, T., Krautz, R., Markus, R., Volkenhoff, A., Kucerova, L., and Theopold, U. (2014). A Drosophila immune response against Ras-induced overgrowth. Biology open *3*, 250-260.
45. Parisi, F., Stefanatos, R.K., Strathdee, K., Yu, Y., and Vidal, M. (2014). Transformed epithelia trigger non-tissue-autonomous tumor suppressor response by adipocytes via activation of Toll and Eiger/TNF signaling. Cell reports *6*, 855-867.
46. Pastor-Pareja, J.C., Wu, M., and Xu, T. (2008). An innate immune response of blood cells to tumors and tissue damage in Drosophila. Disease models & mechanisms *1*, 144-154; discussion 153.

47. Ayyaz, A., Li, H., and Jasper, H. (2015). Haemocytes control stem cell activity in the Drosophila intestine. Nature cell biology *17*, 736-748.
48. Biswas, S.K., Allavena, P., and Mantovani, A. (2013). Tumor-associated macrophages: functional diversity, clinical significance, and open questions. Seminars in immunopathology *35*, 585-600.
49. Dvorak, H.F. (1986). Tumors: wounds that do not heal. Similarities between tumor stroma generation and wound healing. The New England journal of medicine *315*, 1650-1659.
50. Makhijani, K., Alexander, B., Tanaka, T., Rulifson, E., and Bruckner, K. (2011). The peripheral nervous system supports blood cell homing and survival in the Drosophila larva. Development *138*, 5379-5391.

Figure 1: Ectopic Production of Reactive Oxygen Species (ROS) in Apoptosis-induced Proliferation (AiP). (See also Figures S1 and S2).

(A,B) Representative examples of adult heads of control (*ey>p35*) and experimental (undead: *ey>hid-p35*) animals. The latter are characterized by overgrowth with duplications of bristles (arrows) and ocelli (arrowhead), often at the expense of eye size. Scale bars: 200 μm.

(C) Heterozygosity of *dronc* suppresses overgrowth of adult heads of *ey>hid-p35* animals.

(D-F;H-J) Shown are 3rd instar larval eye imaginal discs labeled for ROS with dihydroethidium (DHE) (D-F) and fluorescein based H_2-DCF-DA (H-J). Disc outline is marked by white dashed lines. The yellow dotted lines mark the portion of the eye discs in which *ey-Gal4* is expressed. In (E,I), the anterior portion of the eye disc is composed of undead tissue (*ey>hid-p35*) which is overgrown at the expense of the posterior parts of the disc (see also Figure S1). ROS levels are significantly higher in these overgrown, undead areas compared to control (*ey>p35*) discs (D,H). ROS levels are strongly suppressed in a $dronc^{I29}$ heterozygous background (F,J). Arrows in (E) and (I) indicate ROS in anterior undead tissue. Scale bars 50 μm.

(G,K) Quantification reveals that ROS levels are significantly higher in overgrown, undead discs (*ey>hid-p35*) than control (*ey>p35*) eye imaginal discs, while ROS levels are strongly suppressed in a $dronc^{I29}$ heterozygous background. Quantification over the entire eye disc excluding the antennal disc is signal intensity per μm^2 ±SEM analyzed by one-way ANOVA, with Holm-Sidak test for multiple comparisons. * p= 0.031 (G) and * p=0.010 (K). n.s.= no statistically significant difference between control and suppressed states. Between 15 and 25 discs of each genotype were analyzed.

(L-O) ROS are detected in an undead wing (*nub>hid-p35*) AiP model (L,M) and a *p35*-independent (regenerative) eye model (*DE^{ts}-hid*) of AiP (N,O). (L) and (N) are the controls for (M) and (O), respectively. The yellow dotted lines indicate the *Gal4* expressing areas which express the indicated transgenes and are marked by GFP (green). ROS are generated within the domains of specific cell death induction (arrows in M' and O'). Genotypes are indicated above the panels. Scale bars 50 μm.

Figure 2: Extracellular ROS are required for AiP upstream of JNK. (See also Figures S3 and S4).

(A-D) Reduction of extracellular ROS suppresses overgrowth. Representative examples of adult heads obtained from *ey>hid-p35* animals overexpressing the indicated reducing enzymes or RNAi against the ROS producing enzymes Nox or Duox . Expression of *IRC* (B) and *Duox^{RNAi}* (D) suppresses overgrowth of adult heads of *ey>hid-p35* animals. Scale bars = 200μm.

(E) Summary of the results regarding overexpression of catalases and SOD as well as RNAi-mediated knockdown of the NADPH oxidases Nox and Duox. Based on qualitative screening criteria (presence of ectopic ocelli and bristles; expansion of mid-head capsule width; see Figure 1B), progeny are scored as wild type (black bars) or having an overgrowth phenotype (red bars). Suppression is determined based on a shift in the percentage to wild-type from overgrown animals that is significantly different based on a Pearson's chi-squared test for degrees of freedom=1, $\chi^2 = 10.83$ at p=0.001. Strong suppressors may also increase the overall survival as the *ey>hid-p35* genotype is associated with ~50% lethality, whereas enhancers may decrease survival to adulthood (increased lethality). See also detailed statistical analysis in Figure S3F.

(F) Quantification of the PH3 labelings in (G-I). The number of mitotic cells in undead tissue (*ey>hid-p35*) is significantly reduced after ROS removal through *Duox*^{RNAi} and *hCatS* expression and equals control levels (*ey>p35*). Quantification over the entire eye disc excluding the antennal disc is number of PH3-positive cells analyzed by one-way ANOVA, with Holm-Sidak test for multiple comparisons. *** $p<0.001$ and ** $p<0.01$. Seven discs per genotype were analyzed.

(G-I) In larval eye imaginal *ey>hid-p35* discs, RNAi against the ROS-producing *Duox* (H) and transgenic expression of the human catalase *hCatS* (I) results in suppression of JNK activity (measured by MMP1; red in G-I; grey in G'-I'; see arrows) in the anterior undead eye tissue (between the yellow dotted lines). PH3 labeling (G"-I") revealed a significant decrease of cell proliferation after reduction of extracellular ROS by *Duox*^{RNAi} and *hCatS* overexpression. Quantified in (F). Scale bars 50 μm.

Figure 3: ROS activate Hemocytes for Apoptosis-induced Proliferation. (See also Figure S5).

In (A,B,E,F), the *ey-Gal4* expressing areas in the anterior portion of the larval eye imaginal discs which corresponds to undead tissue in (B,E,F), lies between the yellow dotted lines. Hemocytes are detected by the pan-hemocyte specific antibody anti-Hemese (red in A,B,E,F; grey in (A',B',C',D'). In (C,D), hemocytes are labeled using the plasmatocyte-specific anti-NimC antibody. Cleaved Caspase 3 (CC3) antibody labeling is shown in green (A,B,E,F) and grey (A",B",C",D"). Scale bars: 50 μm.

(A) In *ey>p35* control discs, hemocytes (red in A; grey in A') are found in a clumped aggregate pattern along the boundary between anterior proliferating and posterior differentiating eye tissue

(visualized by ELAV labeling in blue (A); separated by the right yellow dotted line). They are also present as a cell aggregate in the antennal portion of the imaginal disc (left). CC3 labeling is not detectable in these control discs (A")

(B) Hemocytes adhere as single cells or small cell clusters on undead *ey>hid-p35* eye tissue with reduced spherical morphology (B'). They are present in overgrown areas which in this case extend into the posterior portion of the disc as visualized by the disrupted ELAV pattern (blue). There is strong CC3 labeling in this portion of the eye discs (B").

(C) Hemocytes (NimC) are attached to control discs as large cell aggregates.

(D) Hemocytes (NimC) attached to undead tissue extent protrusions (arrows), making extensive contacts with the epithelial layer of the imaginal disc.

(E,F) Hemocyte association with *ey>hid-p35* eye disc is abolished or reduced to control levels upon loss of ROS by transgenic expression of $Duox^{RNAi}$ (E) and *hCatS* (F). The ELAV pattern is normalized in these discs (blue in E, F) indicating suppression of abnormal growth. CC3 labeling is reduced, but not absent, in (E",F") compared to *ey>hid-p35* discs alone (B").

Figure 4: Hemocytes are required for AiP-induced overgrowth. (See also Figures S3 and S6).

(A-D) Representative examples of adult heads of *ey>hid-p35* animals that are either wild-type (A), heterozygous for two *serpent* (*srp*) alleles (B,C) or express *UAS-*srp^{RNAi} transgenes (D). The *srp* alleles used are indicated above the panels. The srp^{RNAi} line used in (D) is BL34080 from

Bloomington Stock center. Similar data were obtained for two additional srp^{RNAi} stocks (see E). Scale bars: 200 μm.

(E) Schematic representation of the effects of *srp* alleles and *srp* RNAi on the *ey>hid-p35* overgrowth phenotype. Based on qualitative screening criteria (presence of ectopic ocelli and bristles; expansion of mid-head capsule width; see Figure 1B), progeny are scored as wild type (black bars) or having an overgrowth phenotype (red bars). Suppression is determined based on a shift in the percentage to wild-type from overgrown animals that is significantly different based on a Pearson's chi-squared test for degrees of freedom=1, $\chi^2 = 10.83$ at p=.001. See Figure S3G for detailed statistical analysis.

(F,G,H) *srp* alleles strongly suppress JNK activity in larval eye imaginal discs. Yellow dotted lines mark the undead tissue (arrows). MMP1 labeling (red in F,G,H; grey in F',G',H') was used as a JNK activity marker. ELAV labeling (blue) indicates normalization of eye disc patterning by heterozygous *srp* alleles. Scale bars 50 μm.

(I,J,K) CC3 is reduced, but not absent, by *srp* alleles (green in I-K; grey in I'-K') suggesting that hemocytes participate in the feedback amplification loop in apoptotic cells. As shown in (F-H), the ELAV (blue) pattern is normalized. Yellow dotted lines mark the undead tissue (arrows). Scale bars 50 μm.

Figure 5: Hemocytes activate JNK through the TNF system Eiger/Grindelwald. (See also Figure S3).

(A) Shown is a mildly overgrown *ey>hid-p35* larval eye-antennal imaginal disc. Dashed white lines outline the disc, while the undead tissue is located between the yellow dotted lines. Hemocytes are labeled with nuclear *hml Δ RFP* marker (red) [50] and JNK activity is shown by *puc-lacZ* staining (white). Activated hemocytes are present as single cells (white arrow), while inactive hemocytes form cell clusters in the antennal portion of the disc and in the posterior eye disc (red arrows). Only activated hemocytes are found directly adjacent to *puc-lacZ*-positive epithelial cells in undead tissue. The white arrow in (A) indicates the location where the orthogonal (YZ) section was applied, shown enlarged in (A'). Yellow arrows in (A') highlight examples where hemocytes are adjacent to *puc-lacZ*-positive epithelial cells. Scale bar 50 μm.

(B-D) *eiger* (*egr*) mutants (C) and eye-specific (*ey-Gal4*) knockdown of *grindelwald* (*grnd*) (D) strongly suppress the overgrowth of the adult head cuticle of *ey>hid-p35* animals (B). Genotype in (C): *UAS-hid*; egr^3/egr^3; *ey-Gal4 UAS-p35*. Scale bars 200 μm.

(E) Quantification of the suppression of overgrowth of *ey>hid-p35* animals by egr^3 mutants, *egr* RNAi, *wengen* (*wgn*) RNAi and *grindelwald* (*grnd*) RNAi. Based on qualitative screening criteria (presence of ectopic ocelli and bristles; expansion of mid-head capsule width; see Figure 1B), progeny are scored as wild type (black bars) or having an overgrowth phenotype (red bars). Suppression is determined based on a shift in the percentage to wild-type from overgrown animals that is significantly different based on a Pearson's chi-squared test for degrees of freedom=1, $\chi^2 = 10.83$ at p=.001. For detailed statistical analysis see Figure S3H.

(F,G,H) *eiger* mutants suppress JNK activity in *ey>hid-p35* discs. Dashed white lines outline the disc, while the undead tissue is located between the yellow dotted lines. The suppression of adult head overgrowth of *ey>hid-p35* animals by *egr* mutants (C) correlates with loss of JNK

activity (MMP1; red in F-H; grey in F'-H'; see arrows) and normalization of the ELAV pattern (blue) in *ey>hid-p35* discs (compare G and H). Scale bars 50 μm.

(I) *grnd* RNAi suppresses JNK activity (*puc-lacZ*) in undead tissue (between yellow dotted lines, see arrow in I') suggesting that Grnd is required for JNK activation. The suppression of adult head overgrowth by *Grnd* RNAi correlates with normalization of the ELAV pattern (magenta) in *ey>hid-p35* tissue. CC3 (green) labeling is present, but reduced, in *ey>hid-p35; Grnd* RNAi discs. Scale bar 50 μm.

Figure 6: Hemocytes are a source of the TNF ligand Eiger.

Shown are eye-antennal imaginal discs from third instar larvae labeled with anti-Eiger antibody (red) and NimC antibody (green) to identify hemocytes (plasmatocytes). Scale bars 50 μm.

(A,B) Anti-Eiger labeling (red) of control (*ey>p35*) eye discs with attached hemocytes (green). Inset from (A) is magnified in (B). Yellow line in (B) marks the orthogonal (YZ) section shown in (B'). Diffuse Eiger staining is seen in disc epithelium, but not in hemocytes (B").

(C,D) Anti-Eiger labeling of undead (*ey>hid-p35*) eye discs with attached hemocytes (green). Inset from (C) is magnified in (D). Yellow line in (D) marks the orthogonal (YZ) section shown in (D'). At higher magnification, increased Eiger labeling can be seen in hemocytes in the overgrown region of an undead disc (arrows in D,D',D") as well as at epithelial cells close to hemocytes (arrowhead in D and D").

Figure 7. Schematic summary of the AiP events presented in this work.

ey-Gal4 driven Hid in undead cells triggers a feedback amplification loop that involves Duox, ROS, hemocytes and Eiger signaling, ultimately resulting in AiP. JNK feeds back on endogenous Hid [20, 37] which maintains the amplification loop. Depending on the location of hemocytes on the imaginal disc, either undead or neighboring normal epithelial cells receive the Eiger signal for JNK activation. All proteins highlighted in yellow are required for AiP. The red arrows indicate participation in the feedback amplification loop. Dotted lines and question marks indicate uncertainty. Not drawn to scale. In fact, hemocytes are much larger than epithelial disc cells.

Figure 1

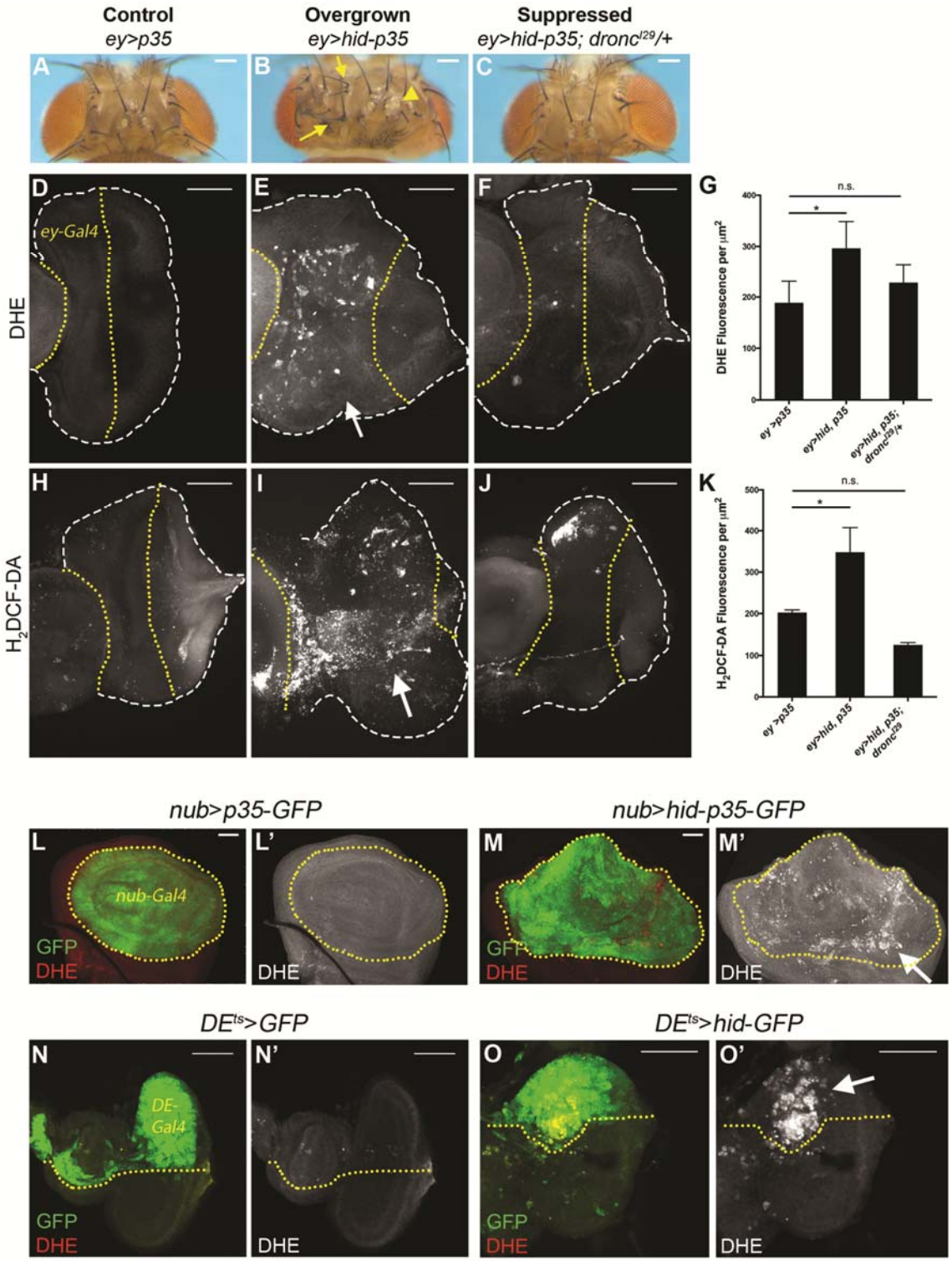
Control
ey>p35
Overgrown
ey>hid-p35
Suppressed
ey>hid-p35; dronc^I29/+
A
B
C
D
E
F
G
ey-Gal4
DHE
DHE Fluorescence per μm²
n.s.
*
ey >p35
ey>hid, p35
ey>hid, p35; dronc^I29/+
H
I
J
K
H2DCF-DA
H2DCF-DA Fluorescence per μm²
ey >p35
ey>hid, p35
ey>hid, p35; dronc^I29
nub>p35-GFP
nub>hid-p35-GFP
L
L'
M
M'
nub-Gal4
GFP
DHE
DE^ts>GFP
DE^ts>hid-GFP
N
N'
O
O'
DE-Gal4

Figure 2

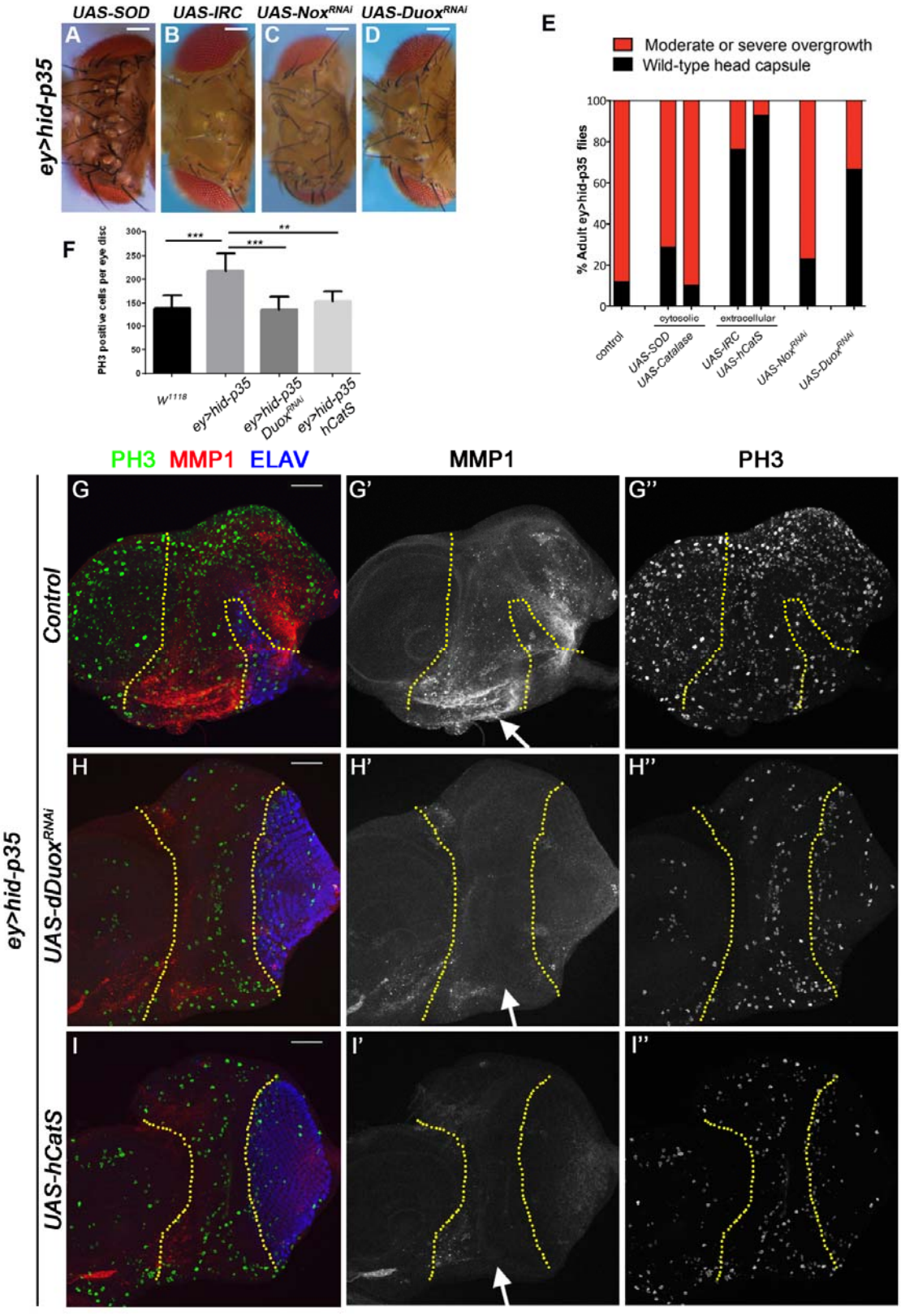
UAS-SOD
UAS-IRC
UAS-Nox^RNAi
UAS-Duox^RNAi
A
B
C
D
ey>hid-p35
E
Moderate or severe overgrowth
Wild-type head capsule
% Adult ey>hid-p35 flies
100
80
60
40
20
0
cytosolic
extracellular
control
UAS-SOD
UAS-Catalase
UAS-IRC
UAS-hCatS
UAS-Nox^RNAi
UAS-Duox^RNAi
F
PH3 positive cells per eye disc
300
250
200
150
100
50
0
***
***
**
w^1118
ey>hid-p35
ey>hid-p35 Duox^RNAi
ey>hid-p35 hCatS
PH3 MMP1 ELAV
MMP1
PH3
G
G'
G''
H
H'
H''
I
I'
I''
Control
UAS-dDuox^RNAi
UAS-hCatS
ey>hid-p35

Figure 3

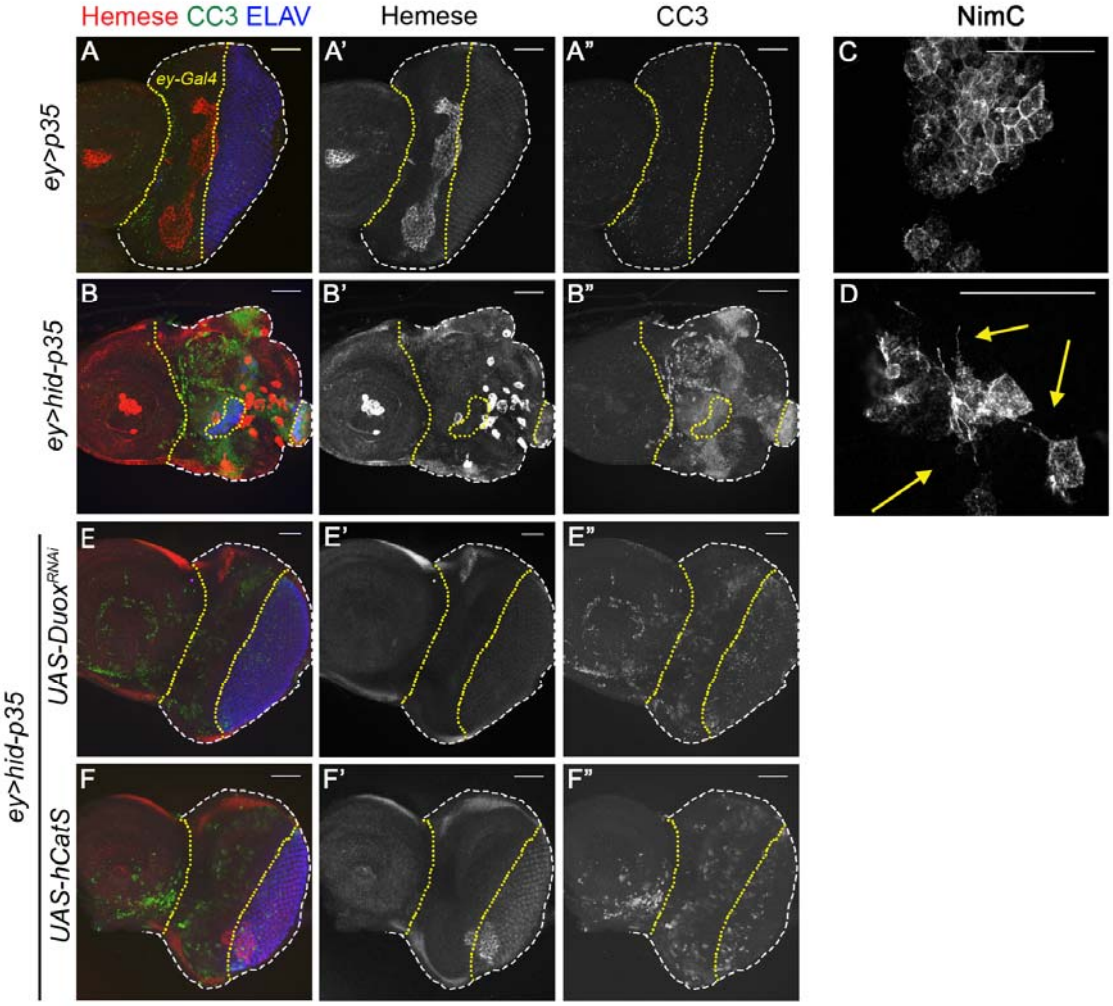
Hemese CC3 ELAV
Hemese
CC3
NimC
A
A'
A"
C
ey-Gal4
ey>p35
B
B'
B"
D
ey>hid-p35
E
E'
E"
UAS-Duox^RNAi
F
F'
F"
UAS-hCatS
ey>hid-p35

Figure 4

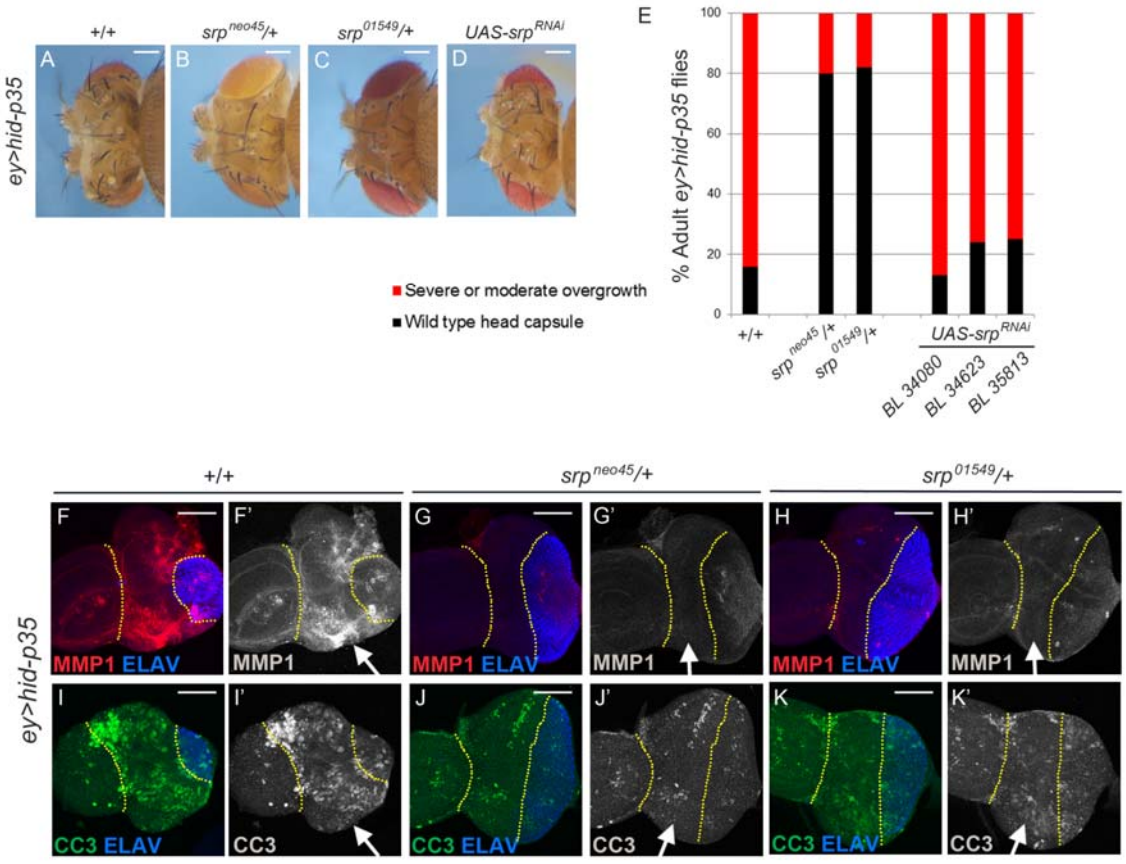
+/+
srp neo45/+
srp 01549/+
UAS-srp RNAi
A
B
C
D
ey>hid-p35
Severe or moderate overgrowth
Wild type head capsule
E
% Adult ey>hid-p35 flies
100
80
60
40
20
0
+/+
srp neo45 /+
srp 01549/+
UAS-srp RNAi
BL 34080
BL 34623
BL 35813
+/+
srp neo45/+
srp 01549/+
F
F'
G
G'
H
H'
MMP1 ELAV
MMP1
I
I'
J
J'
K
K'
CC3 ELAV
CC3
ey>hid-p35

Figure 5

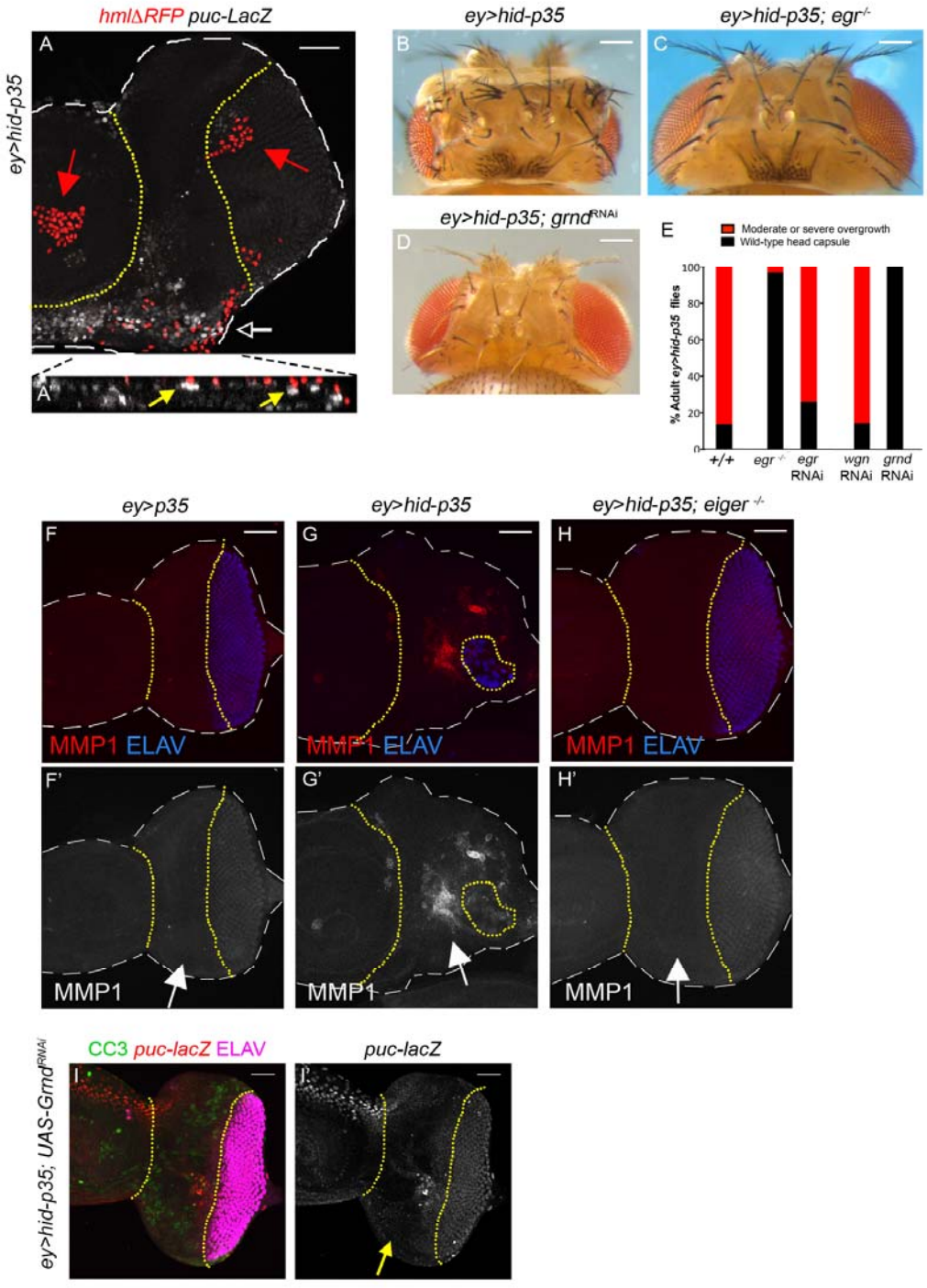
hmlΔRFP puc-LacZ
ey>hid-p35
A
A'
ey>hid-p35
B
ey>hid-p35; egr-/-
C
ey>hid-p35; grndRNAi
D
E
Moderate or severe overgrowth
Wild-type head capsule
% Adult ey>hid-p35 flies
100
80
60
40
20
0
+/+
egr-/-
egr RNAi
wgn RNAi
grnd RNAi
ey>p35
ey>hid-p35
ey>hid-p35; eiger-/-
F
G
H
MMP1 ELAV
F'
G'
H'
MMP1
ey>hid-p35; UAS-GrndRNAi
CC3 puc-lacZ ELAV
puc-lacZ
I
J

Figure 6

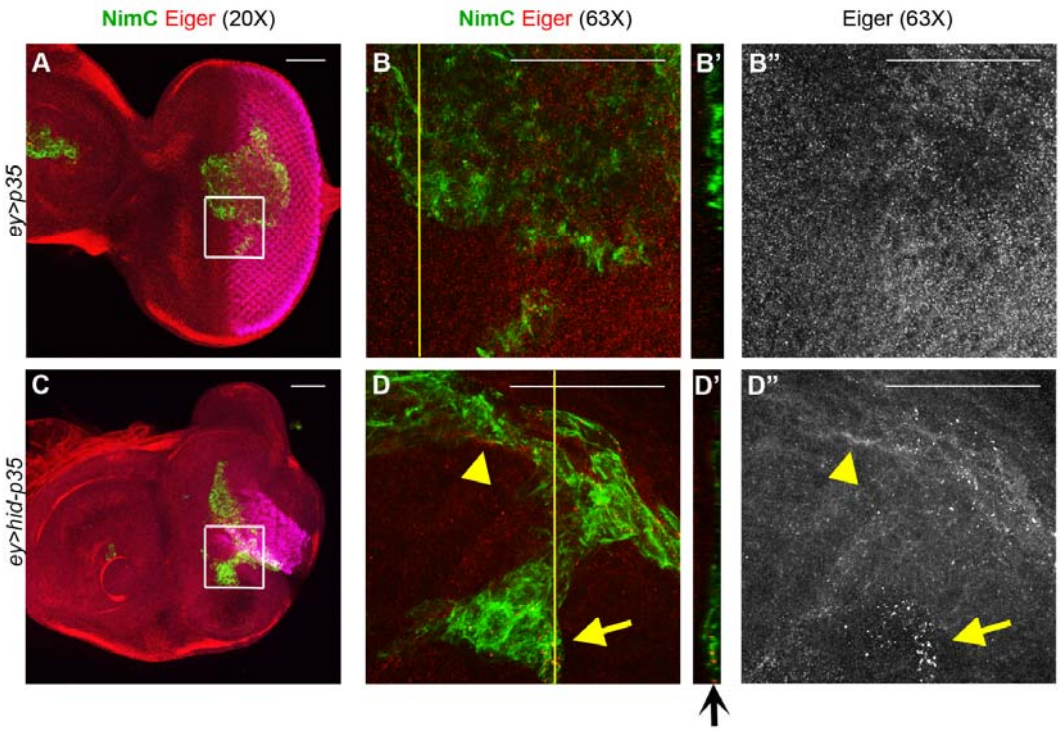
NimC Eiger (20X)
NimC Eiger (63X)
Eiger (63X)
A
B
B'
B"
C
D
D'
D"
ey>p35
ey>hid-p35

Figure 7

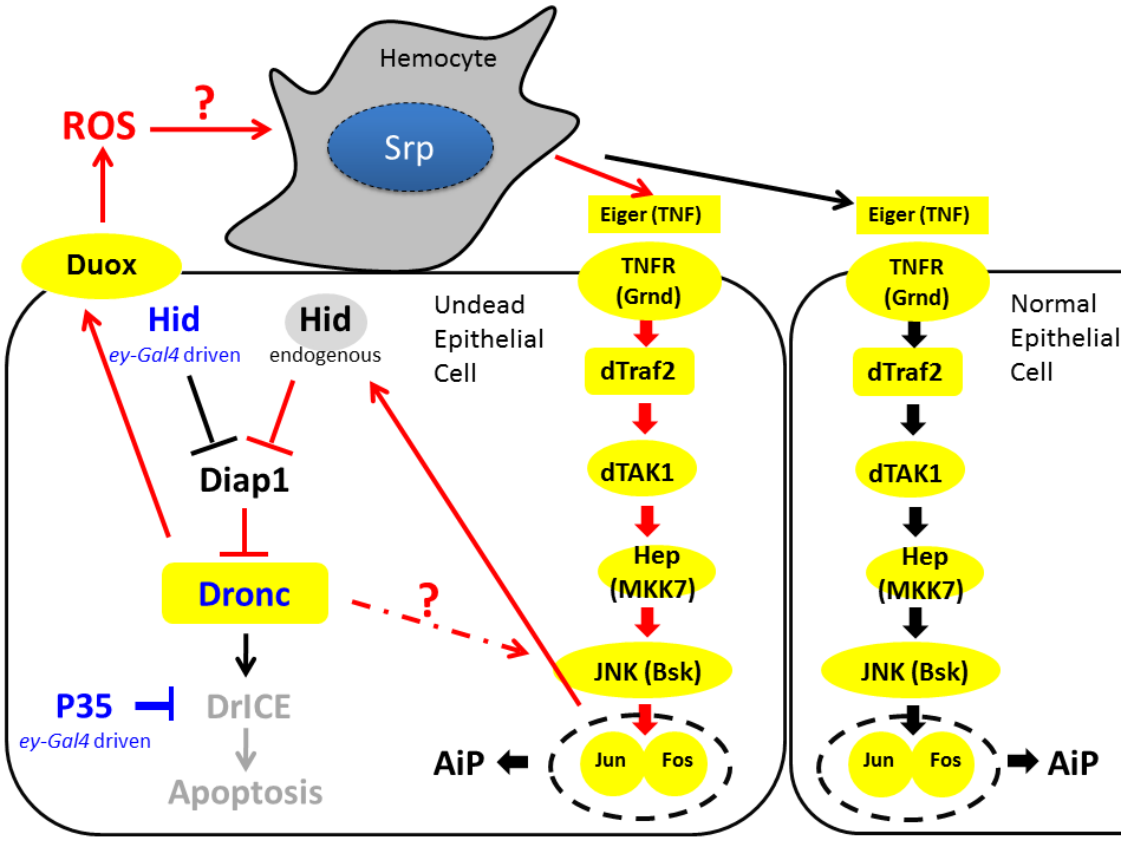
Hemocyte
Srp
ROS
?
Duox
Eiger (TNF)
Eiger (TNF)
TNFR (Grnd)
TNFR (Grnd)
Undead Epithelial Cell
Normal Epithelial Cell
Hid
ey-Gal4 driven
Hid
endogenous
dTraf2
dTraf2
Diap1
dTAK1
dTAK1
Hep (MKK7)
Hep (MKK7)
Dronc
?
JNK (Bsk)
JNK (Bsk)
P35
ey-Gal4 driven
DrICE
Apoptosis
AiP
Jun
Fos
Jun
Fos
AiP

Supplemental Figures

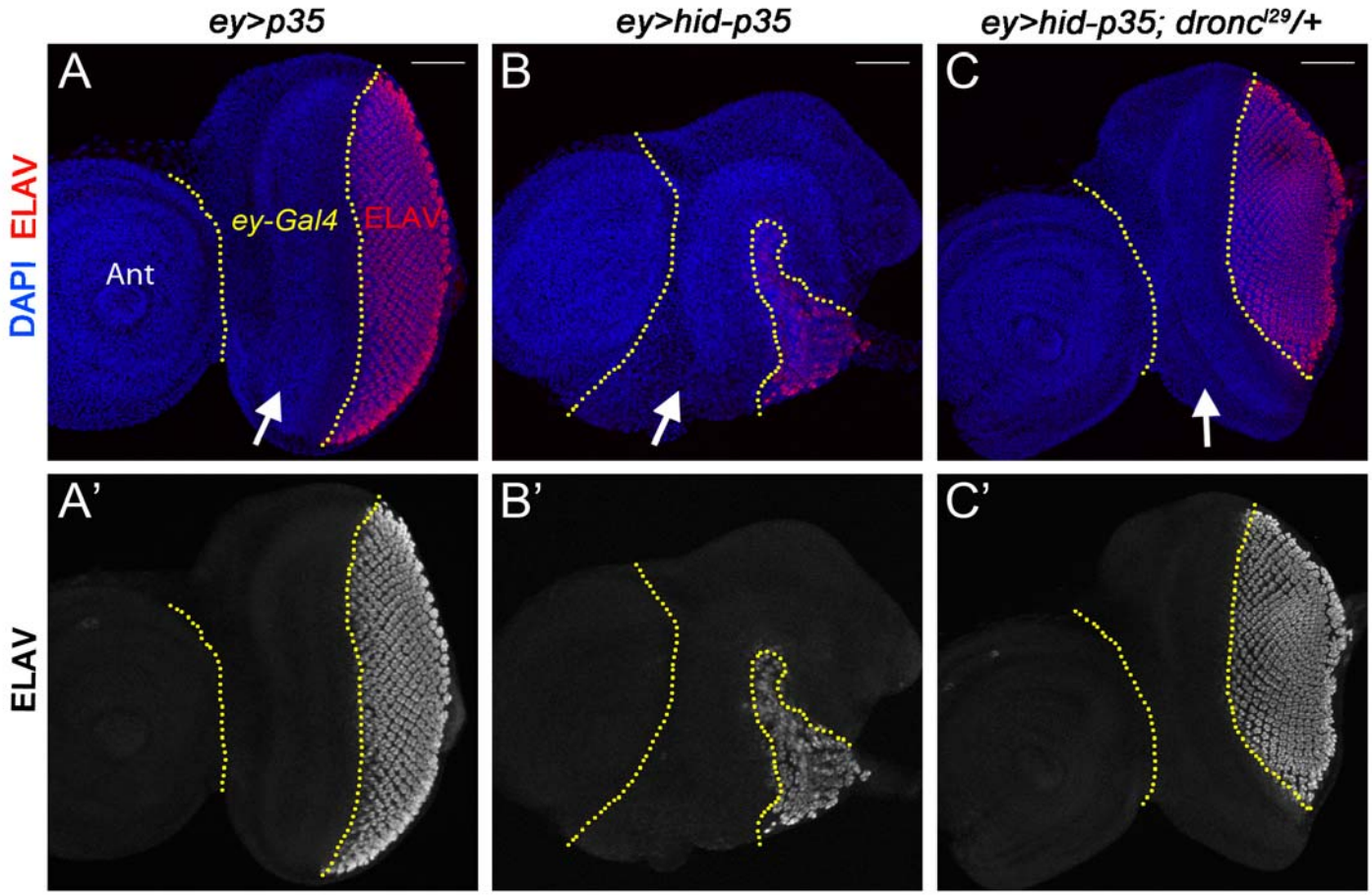

Figure S1. Undead cells in the eye imaginal disc overgrow the posterior eye field which can be suppressed (normalized) by heterozygous *dronc* mutations. (Related to Figure 1)

Shown are 3rd instar larval eye-antennal imaginal discs, outlined by DAPI labeling (blue). The antennal disc (Ant) is to the left. The *ey-Gal4* expressing domain is in the anterior portion of the eye disc (marked by the yellow dotted lines; see white arrows) and corresponds to undead tissue in (B). The posterior portion of the eye disc which does not express *ey>Gal4*, is marked by expression of the photoreceptor marker ELAV (red) and gives rise to the eye field of the disc.

(A) A *ey>p35* control disc. Ant (antennal), *ey-Gal4* (white arrow) and ELAV mark the different parts of the eye-antennal imaginal disc, separated by yellow dotted lines.

(B) In *ey>hid-p35* discs, *ey-Gal4* drives *hid* and *p35* expression in the anterior portion of the eye disc which overgrows and displaces the posterior eye field as visualized by ELAV (red). The white arrow highlights the undead *ey-Gal4* domain which is overgrown at the expense of the posterior eye field as visualized by ELAV. The contour of the discs (blue) is deformed and multi-layered which causes folding.

(C) *dronc*^{I29} heterozygosity in *ey>hid-p35* background normalizes disc morphology (blue) and ELAV pattern (red).

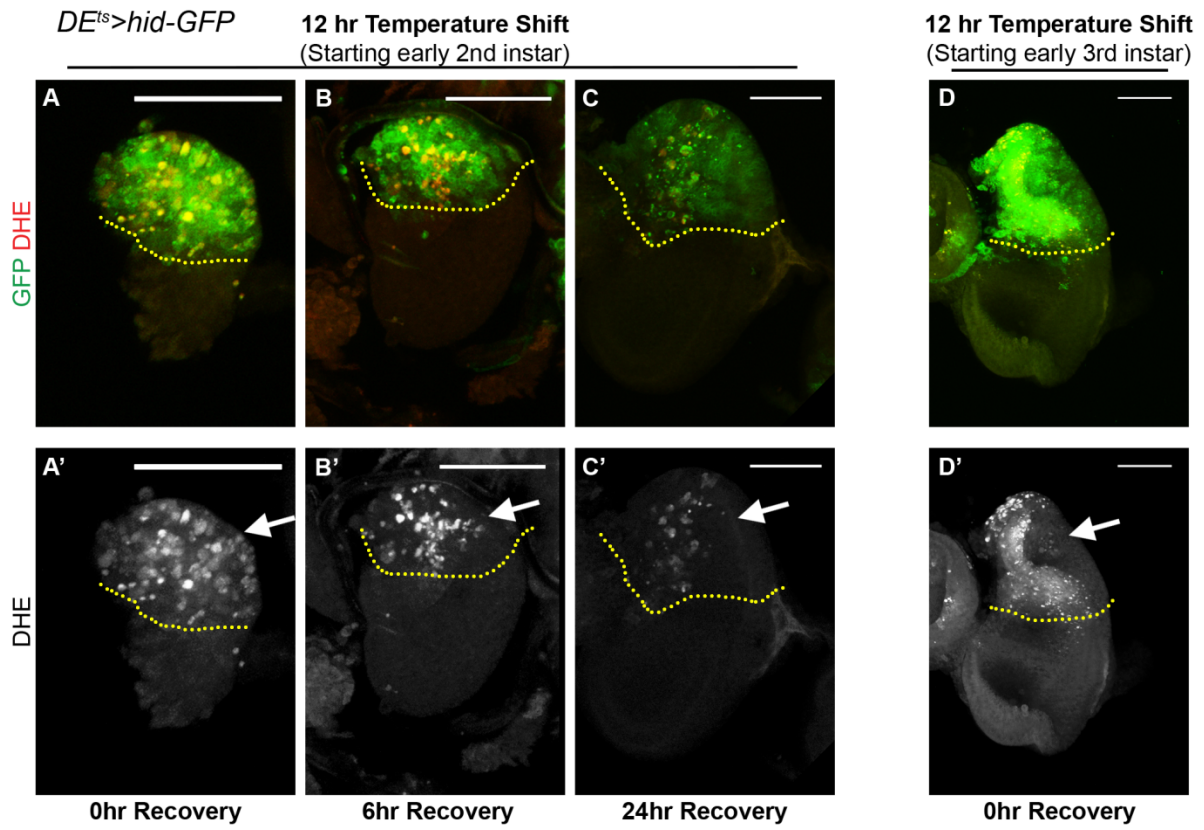

Figure S2. ROS production in a *p35*-independent model of AiP. (Related to Figure 1)

In this model, *hid* expression is restricted to a 12 hour interval in the dorsal half of the eye imaginal disc by *Gal80^{ts}*-controlled *dorsal eye-Gal4* (*DE^{ts}-hid*) activity as described [S1]. ROS are induced within the domains of specific cell death induction, marked by GFP. The yellow dotted lines separate the expression of *hid* in the GFP domain from the internal control at the ventral side. Scale bars 50 μm.

(A-C) ROS are detected by dihydroethidium (DHE; arrows in A'-C') in the death domain of *DE^{ts}>hid* eye imaginal discs immediately after a 12 hour pulse of *hid* induction and persist throughout the death phase up to 24 hours after *hid* induction. The death domain is labeled by GFP (green).

(D) The ROS production is independent of the timing of *hid* induction (2nd (A) vs 3rd (D)) instar of larval development.

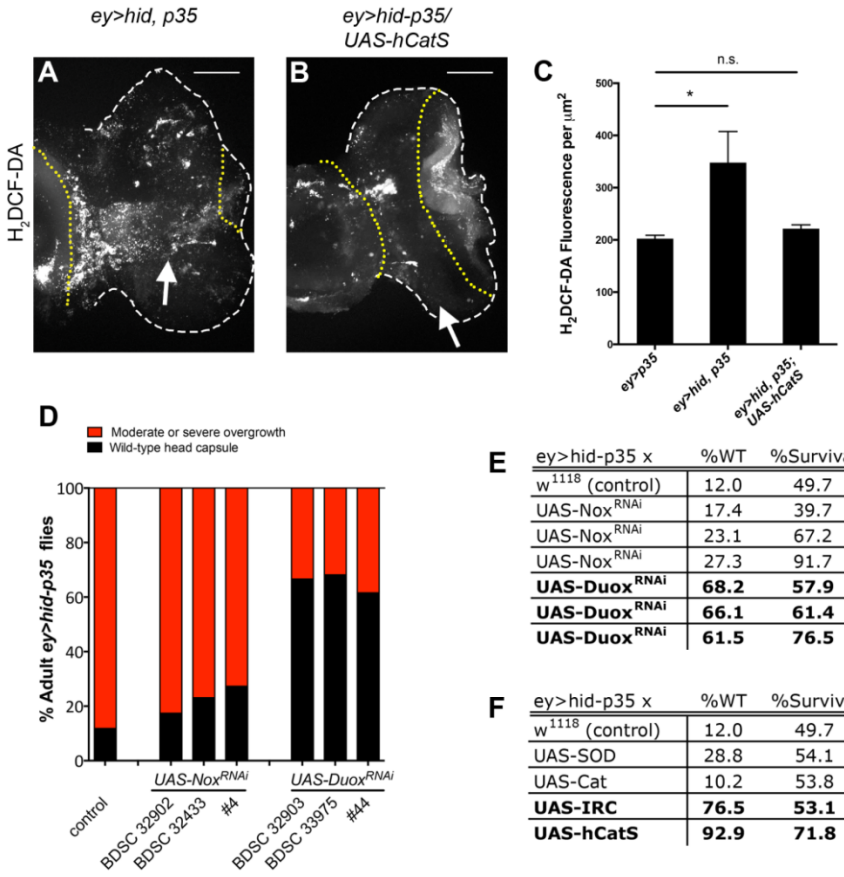

E

ey>hid-p35 x	%WT	%Survival	p<0.001	n
w^{1118} (control)	12.0	49.7	NS	151
UAS-Nox^{RNAi}	17.4	39.7	NS	81
UAS-Nox^{RNAi}	23.1	67.2	NS	97
UAS-Nox^{RNAi}	27.3	91.7	NS	70
UAS-$Duox^{RNAi}$	**68.2**	**57.9**	***	**120**
UAS-$Duox^{RNAi}$	**66.1**	**61.4**	***	**163**
UAS-$Duox^{RNAi}$	**61.5**	**76.5**	***	**94**

F

ey>hid-p35 x	%WT	%Survival	p<0.001	n
w^{1118} (control)	12.0	49.7	NS	151
UAS-SOD	28.8	54.1	NS	336
UAS-Cat	10.2	53.8	NS	140
UAS-IRC	**76.5**	**53.1**	***	**98**
UAS-hCatS	**92.9**	**71.8**	***	**67**

G

ey>hid-p35 x	%WT	%Survival	p<0.001	n
w^{1118} (control)	15.9	66.0	NS	315
srp^{neo45}	**80.0**	**75.0**	***	**53**
srp^{01549}	**87.2**	**80.0**	***	**59**
UAS-srp^{RNAi}	13.5	70.0	NS	74
UAS-srp^{RNAi}	20.2	78.0	NS	146
UAS-srp^{RNAi}	27.2	72.0	NS	143

H

ey>hid-p35 (III) x	%WT	%Survival	p<0.001	n
w^{1118} (control)	13.6	76.0	NS	811
UAS-$Eiger^{RNAi}$	26.0	77.0	NS	418
$Eiger^{-/-}$	**96.9**	**78.0**	***	**167**
UAS-$Wengen^{RNAi}$	14.3	79.0	NS	135
UAS-$Grindelwald^{RNAi}$	**100.0**	**80.0**	***	**432**

Figure S3: Reduction of ROS levels suppresses overgrowth. (Related to Figures 2, 4 and 5)

(A,B,C) ROS levels in *ey>hid-p35* discs are strongly reduced by transgenic expression of human secreted catalase (*hCatS*) (A,B). Dashed white lines outline the disc, while the undead tissue is located between the yellow dashed lines (white arrows). Scale bars 50 µm. (C) Quantifications of the ROS signal intensity per μm^2 ±SD analyzed by one-way ANOVA, with Dunnett's test for multiple comparisons, *p<0.05. (Related to Figure 2A-E)

(D) Three independent transgenes for each of Nox and Duox gave consistent results. The numbers refer to the stock numbers of the Bloomington *Drosophila* Stock Center (BDSC). Lines #4 and #44 were provided by Won Jae Lee. (Related to Figure 2E)

(E-H) Summary of statistical analysis of the suppression assay of *ey>hid-p35* animals by various mutants and RNAi lines. Suppression is determined based on a shift in the percentages of the observed phenotypes, from overgrowth to wild-type (wt), that is significantly different based on a Pearson's chi-squared test (degrees of freedom=1, $\chi^2 = 10.83$ at p=0.001, expected values for phenotypes derived from replicate controls). Shown is the percentage of *ey>hid-p35* animals with wt adult head phenotype. A p-value of <0.001 is marked by ***. Significant suppressors are highlighted in bold. NS – not significant. n indicates the total number of animals scored for each genotype. Shown is also the percentage of surviving animals as the *ey>hid-p35* genotype is associated with ~30-50% lethality. Strong suppressors may also increase the overall survival (% of expected animals that reached eclosion, % viability). (Related to Figures 2E, 4E, 5E)

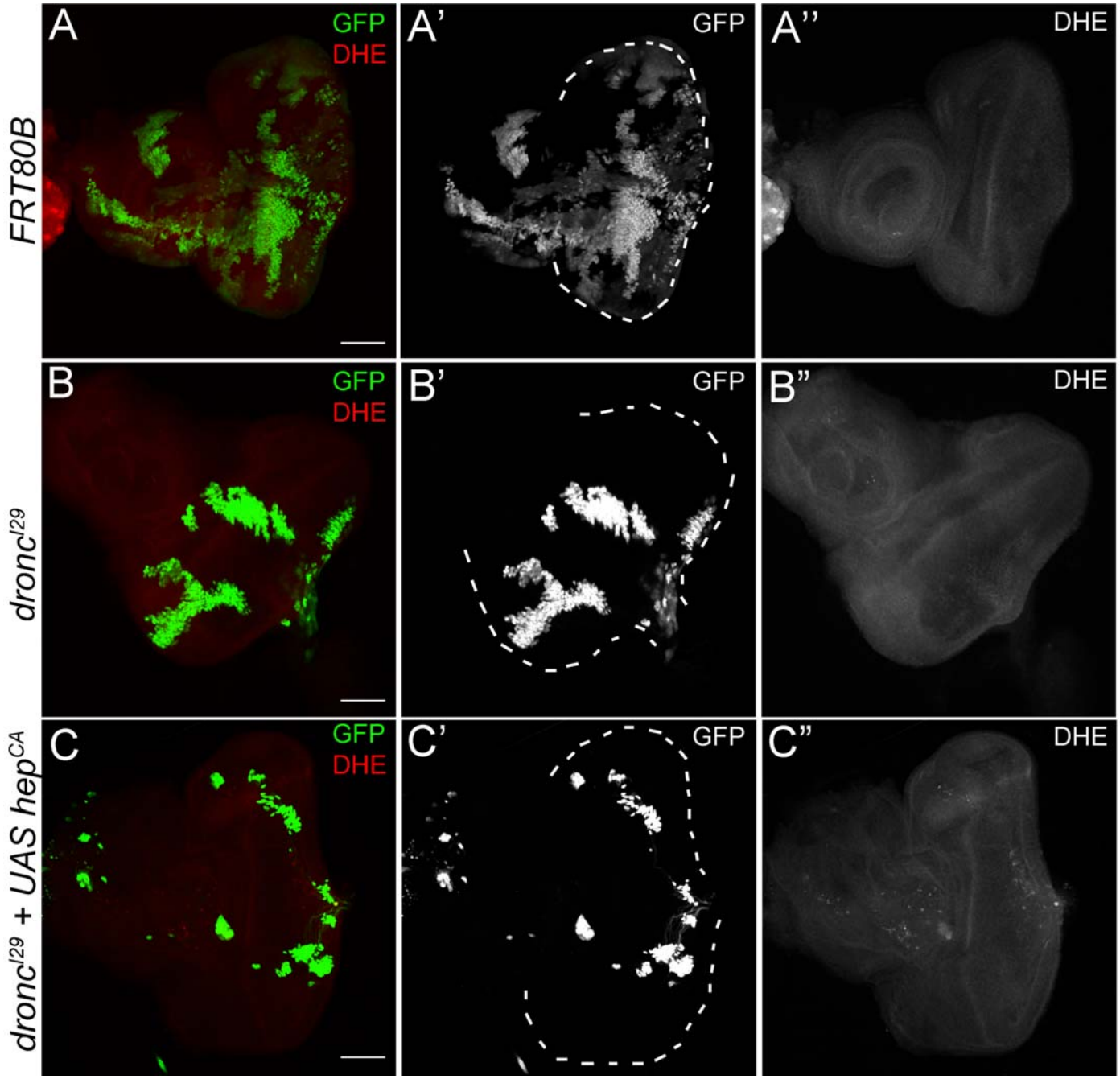

Figure S4. Activation of JNK signaling in *dronc* mutant background is not sufficient to generate ROS. (Related to Figure 2)

(A, B) MARCM clones in the eye disc marked by GFP for control (A) and for $dronc^{I29}$ mutants (B). ROS are not produced in absence of *dronc* as marked by lack of DHE staining (B").

(C-C") Expression of hep^{CA} in *dronc* mutant clones using MARCM clones (marked by GFP) does not lead to ROS production.

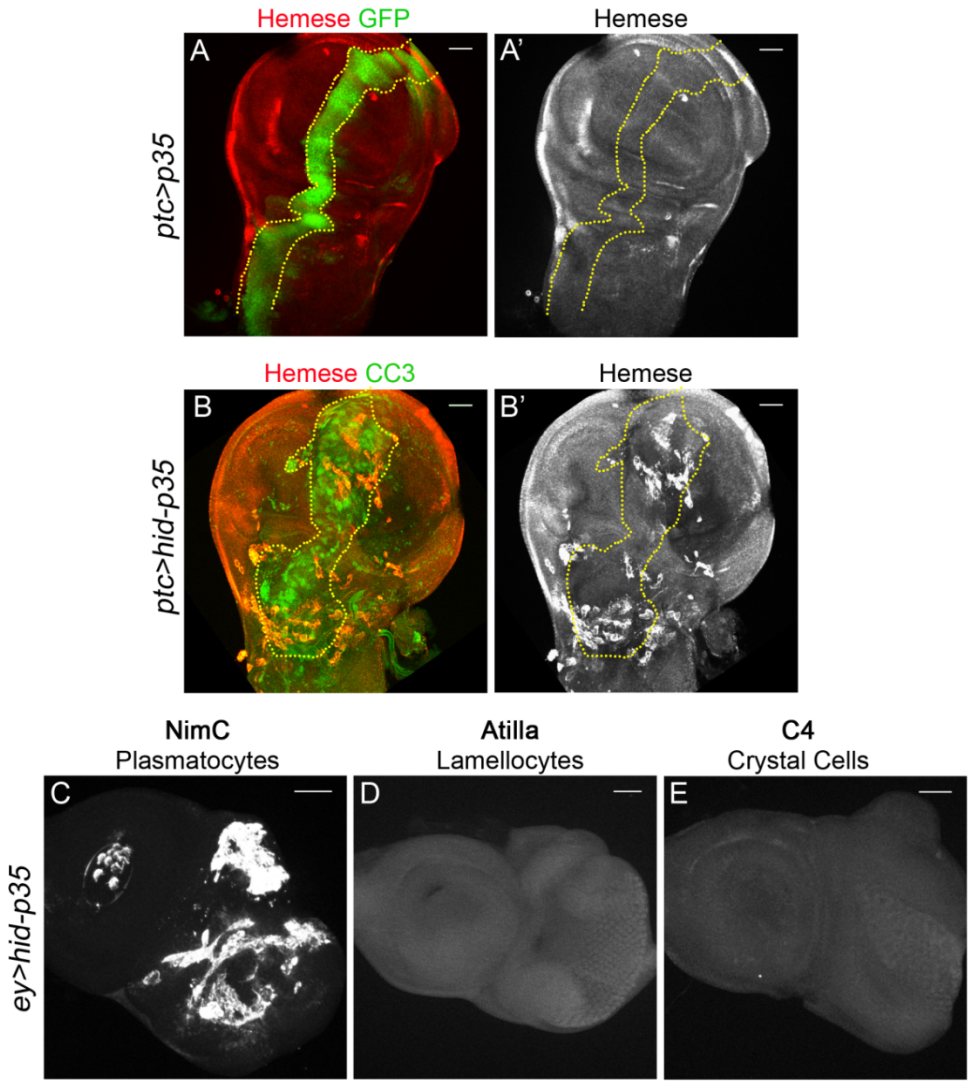

Figure S5: Hemocytes are recruited to undead wing imaginal discs and are plasmatocytes. (Related to Figure 3)

(A) Shown is a *ptc>p35* control wing imaginal disc, labeled with the pan-hemocyte marker Hemese (red in (A) and grey in (A')). Only a few hemocytes are detectable. GFP (green) labels the *ptc* expression domain (yellow dotted lines). Scale bars 50 µm.

(B) Hemocytes (red in (B) and grey in (B')) are recruited in large number to undead wing imaginal discs of genotype *ptc>hid-p35*. They also show similar alterations in morphology as observed in undead eye imaginal discs (Figure 3B,D). Cleaved Caspase 3 (CC3) labeling (green in B; yellow dotted line) is used to mark the undead tissue. Hemocytes attach to the undead portion of the wing tissue. Scale bars 50 µm.

(C-E) Undead (*ey>hid-p35*) eye discs were labeled with plasmatocyte (NimC), lamellocyte (Atilla) and Crystal cell (C4) specific markers. Only NimC antibodies label the discs suggesting that plasmatocytes adhere to undead tissue. Scale bars 50 µm.

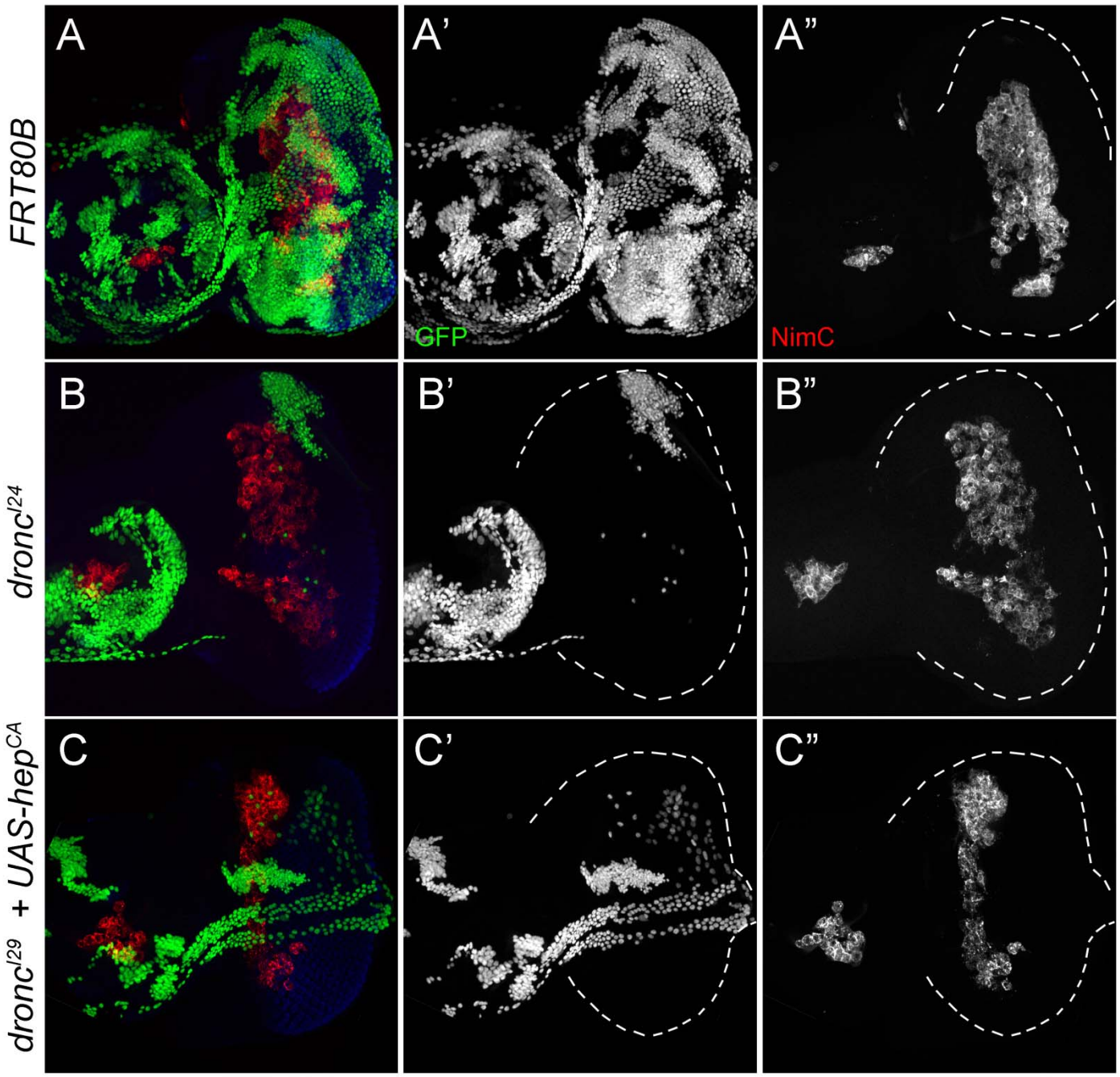

Figure S6. JNK activation in *dronc* mutant background is not sufficient to change hemocyte morphology. (Related to Figure 4)

Hemocytes (marked by NimC, red) on eye discs of control (A-A") and *dronc*^{I24} mutant clones (B-B") appear unaltered for morphology and recruitment. Activation of JNK signaling using activated *hep* (*hep*^{CA}) in mutant background of *dronc* (C-C") does not affect the morphology and/or the recruitment pattern of the hemocytes.

Supplemental Experimental Procedures

Fly stocks

The following mutants and transgenic stocks were used: *dronc*^{I29}; *srp*^{neo45}; *srp*^{01549}; *egr*^{3}; *ey-Gal4*; *ptc-Gal4*; *nub-Gal4*; *DE-Gal4*; *tub-Gal80*^{ts}; *UAS-p35*; *UAS-hid*; *UAS-hep*^{CA}; *puc-lacZ*. *UAS*-based overexpression and RNAi stocks of the following genes were obtained from the stock centers (VDRC, Bloomington and NIG): *SOD1*, *catalase*, *Nox*, *Duox*, *grnd*. *UAS-IRC*, *UAS-hCatS*, *UAS-Duox*^{RNAi} #44, and *UAS-Nox*^{RNAi} #4 were kind gifts from Won Jae Lee. Except where noted, all crosses were maintained at 22°C and controls are crossed to *w*^{1118}. Screening results are presented as the percentage of animals with either wild-type or overgrown phenotype. However, many animals with severe overgrowth do not eclose, therefore the percent survival is also reported as the number eclosed out of a total number expected based on Mendelian ratios (see Figure S3E-H for details).

ROS *in vivo* staining

Imaginal discs and adjacent structures were dissected from 3rd instar larvae (2nd instar for *DE*^{ts}*>hid*) in fresh Schneider's medium for DHE staining and in fresh PBS for H_2-DCF-DA staining, according to the protocol by Owusu-Ansah et al. [S2]. Care was taken to avoid severing the eye imaginal discs from the brain lobes prior to staining, else traumatic injury of the developing photoreceptor axons resulted in excessive signal. Samples were incubated in their respective dyes for 5 minutes, washed, dissected from remaining structures in PBS, mounted in Vectashield mounting media, and imaged immediately on a Zeiss LSM700 confocal microscope. Unless noted all image scale bars represent 50μm. Quantifications of ROS, specifically in the eye region of the eye-antennal disc, are reported as signal per area, determined using ImageJ. Statistical analysis was performed using one-way ANOVA with Dunnett's test for multiple comparisons, α=0.05.

Immunohistochemistry

Imaginal discs were dissected from late 3rd instar larvae, fixed, and stained using standard protocols [S3]. Antibodies to the following primary antigens were used: anti-cleaved Caspase- 3 (Cell Signaling), β-GAL (Promega), PH3 (Millipore), ELAV and MMP1 (DHSB). Anti-Hemese (H2), Nimrod (P1a,P1b), Atilla (L1), and C1 were a kind gift from István Andó [S4]. Anti-Eiger antibody was kindly provided by Masayuki Miura [S5]. Secondary antibodies were donkey Fab fragments from Jackson ImmunoResearch. Images were taken with a Zeiss LSM700 confocal microscope and processed using ImageJ. Unless noted all image scale bars represent 50μm.

Supplemental References

S1. Fan, Y., Wang, S., Hernandez, J., Yenigun, V.B., Hertlein, G., Fogarty, C.E., Lindblad, J.L., and Bergmann, A. (2014). Genetic models of apoptosis-induced proliferation decipher activation of JNK and identify a requirement of EGFR signaling for tissue regenerative responses in Drosophila. PLoS Genetics *10*, e1004131.

S2. Owusu-Ansah, E., Yavari, A., and Banerjee, U. (2008). A protocol for *in vivo* detection of reactive oxygen species. Protocol Exchange doi:10.1038/nprot.2008.23.

S3. Fogarty, C.E., and Bergmann, A. (2014). Detecting caspase activity in Drosophila larval imaginal discs. Methods Mol Biol *1133*, 109-117.

S4. Kurucz, E., Vaczi, B., Markus, R., Laurinyecz, B., Vilmos, P., Zsamboki, J., Csorba, K., Gateff, E., Hultmark, D., and Ando, I. (2007). Definition of Drosophila hemocyte subsets by cell-type specific antigens. Acta biologica Hungarica *58 Suppl*, 95-111.

S5. Igaki, T., Pastor-Pareja, J.C., Aonuma, H., Miura, M., and Xu, T. (2009). Intrinsic tumor suppression and epithelial maintenance by endocytic activation of Eiger/TNF signaling in Drosophila. Dev Cell *16*, 458-465.